Soil Dynamics and Earthquake Engineering 100 (2017) 480–491

Contents lists available at ScienceDirect

Soil Dynamics and Earthquake Engineering

journal homepage: www.elsevier.com/locate/soildyn

Seismic analysis of nailed soil slope considering interface effects

Dhanaji Chavan[a], Goutam Mondal[b], Amit Prashant[c,*]

[a] Indian Institute of Technology Kanpur, India
[b] Indian Institute of Technology Bhubaneswar, India
[c] Indian Institute of Technology Gandhinagar, India

ARTICLE INFO

Keywords:
Nailed soil slope
Earthquake loading
Finite element modelling
Displacement
Soil-nail interface
Overburden pressure

ABSTRACT

Natural soil slopes are often reinforced with nails to stabilize them against earthquake loading. Although pseudo-static method is widely used in designing such slopes; it fails to provide important information such as deformation of slope, effect of soil-nail interface etc. A 2-D finite element model of typical nailed slope has been prepared during this study using OpenSees to perform seismic analysis with due consideration to soil non-linearity, pressure dependency of soil and separation-sliding at soil-nail interface. It is found that the soil-nail interface modelling can significantly influence the permanent deformation of slope after seismic event. The overburden pressure on the nail varies significantly during the earthquake loading and the variation is more when sliding and separation is allowed at the soil-nail interface. It is also found that the model with fixed interface leads to a perception of reinforced soil acting as a relatively rigid block, which results into an unconservative design from overall deformation perspective.

1. Introduction

The seismic stability of in-situ slopes and embankments is often increased by reinforcing them with nails. During 1989 Loma Prieta earthquake, nailed excavations, even in the vicinity of the earthquake epicenter, in the San Francisco Bay area performed exceptionally well although such performance was mainly attributed to the conservative design and stability analysis [1].

Finite element (FE) analysis of slopes is becoming a standard practice as compared to alternative conventional equilibrium methods [2]. Zhang et al. [3] developed a 3-dimensional FE model for static stability analysis of excavated steep slopes and found that there was good agreement between predicted and observed movements. Wang and Richwien [4] studied the soil-nail interface friction and found that the mobilized friction between soil and nail depends upon the dilatancy angle and the elastic parameters of soil. Ann et al. [5] performed 2-D finite element analysis to back analyse the instrumented soil nailed slopes under gravity loading. They felt need of higher order soil and interface models to capture the behavior of nailed soil slopes. Fan and Luo [6] carried out nonlinear finite element analysis, for static loading to determine the optimum layout of nails in slope and found that nails in the lower one-third part of slopes play important role in the stability of slopes. Sahoo et al. [7] carried out 3-D finite element analysis of small and steep nailed soil slopes subjected to earthquake loading using software MIDAS GTS. Interface elements were provided at the soil-nail interface. They studied effect of parameters such as nail inclination, nail length, frequency amplification and slope angle on the seismic resistance and failure mechanism. It was found that the inclined nails offer more resistance to deformation than the horizontal nails. Effect of nail length and amplification factor on the seismic resistance was found to be negligible.

The effect of modelling interface between the nail and soil on the seismic response of the soil-nail system has been explored in the present study. This aspect has remained relatively unexplored in the previous investigations, although it is expected to have significant impact on the overall deformation response of nailed soil slopes. In addition to this, in the conventional Pseudo-static design of nailed soil slopes, the overburden pressure on the nail is assumed to be constant. However, in reality, during the seismic shaking this overburden pressure will vary. Therefore, it becomes essential to study the variation of overburden pressure on the nail and to see how far the assumption is reliable.

In this study, nonlinear finite element analysis of a typical nailed soil slope subjected to earthquake loading has been carried using an open source code OpenSees [8] to investigate the abovementioned issues. Two cases of soil-nail interface modelling have been considered; first with perfect bonding between soil and nail, and second with the sliding and separation allowed at the soil-nail interface. Radiation damping at the boundaries of the model has been incorporated by providing Lysmer boundary [9]. Soil is assumed to be dry and cohesionless, and analyzed under plane strain conditions. The effect of

* Corresponding author.
E-mail addresses: dschavan83@gmail.com (D. Chavan), gmondal@iitbbs.ac.in (G. Mondal), ap@iitgn.ac.in (A. Prashant).

http://dx.doi.org/10.1016/j.soildyn.2017.06.024
Received 5 October 2015; Received in revised form 11 May 2017; Accepted 29 June 2017
Available online 06 July 2017

Nomenclature

A_n	cross sectional area of nail	E_p	modulus of elasticity of plate
A_p	cross sectional area of plate with width equal to spacing S_h of nails	G	shear modulus
E_n	modulus of elasticity of nail	K_N	normal penalty
		K_T	tangential penalty
		S_h	horizontal spacing between nails
		ρ	density of soil

interface modelling on the overall deformation of slope has been discussed in detail.

2. Design of nailed soil slope considered in the study

Fig. 1 shows schematic of the 12 m high soil-slope considered in this study. Soil profile of 62 m depth is rested on bed rock and it consists of three layers; top 12 m of the profile consists of medium sand followed by 20 m thick layer of medium-dense sand overlying 30 m thick layer of dense sand. The inclination of slope from horizontal is 60°. The number and length of the nail to be used in finite element model was obtained after designing the slope using Michalowski's method [10,11] by considering 1940 Imperial valley earthquake loading recorded at CSMIP station number 117 at El Centro site [11]. This method is based on the kinematic limit analysis of geosynthetic reinforced slopes subjected to earthquake loading. In the first step, the minimum strength of reinforcement required to keep slope just stable is worked out by performing upper bound limit analysis, and assuming tensile failure of reinforcement layers. While doing so a log-spiral failure surface which is kinematically admissible is used in the analysis. In the next step, the length of the reinforcement, for a given number of reinforcement layers, is worked out by considering pull-out of some layers and rupture in others. To calculate reinforcement length two types of failure surfaces have been considered; one is rotational and the other sliding. The maximum of two calculated lengths are used in design. Details of the nails provided in the designed slope are given in Table 1.

3. Finite element modelling of soil-nail system

The finite element model of the soil-nail system is described here including material models, finite elements, meshing scheme, boundary conditions, application of earthquake motion, nail-soil interface modelling, verification of model, etc.

3.1. Soil and nail

The overall FE model of the nailed slope is shown in Fig. 2. The soil domain is discretized using four-node quadrilateral elements with four gauss points as shown in Fig. 2a. Each node of the element has two translational degrees of freedom. The constitutive behavior of soil was modeled using a pressure dependent multi-yield (nested yield surface) material model proposed by Iwan [12], Mroz [13], and Prevost [14], and modified later by Parra-Colmenares [15] and Yang [16]. It is a nonlinear elastic-plastic material model that captures the essential characteristics such as dilation (i.e., volume contraction or expansion during shearing), cyclic mobility (i.e., non-flow liquefaction) of sand or silt typically observed during monotonic or cyclic loading. The model has been already calibrated and validated for cyclic loading by Elgamal et al. [17] and Yang et al. [18]. Thus; it is expected to simulate the seismic response of the soil well enough. The detailed description of yield function, hardening rule, and flow rule of the constitutive model can be found elsewhere [15,16]. Table 2 presents the relevant parameters and their values needed for the constitutive model of soil, which were taken from typical values given in the OpenSees Manual [8,19]. The present study considers dry cohesionless soil. The maximum size of element in the direction of propagation of wave was restricted to one eighth to one tenth of the shortest wavelength expected to be traveling through the soil medium [20]. The soil domain was analyzed assuming plane-strain condition.

Nails are the discretely placed elements in three-dimensional (3D) space. In the present study, two-dimensional (2D) plane strain modelling of nailed soil slope was carried out. Therefore, 3D nails were converted to equivalent 2D nails using the equivalent plate approach proposed by Al-Hussaini and Johnson [21]. In this approach, the nails are replaced by a plate of equivalent axial stiffness. The equivalent axial stiffness of plate is obtained using the following equation [22]:

$$E_p = E_n \frac{A_n}{A_p} \tag{1}$$

Where, A_n is cross sectional area of nail, A_p denotes the cross sectional area of plate with width equal to the horizontal spacing (S_h) of nails, E_n and E_p are the Young's modulus of the nails and plates, respectively. The nails were considered to be linear-elastic under earthquake shaking. Therefore, these were modeled as two-node elastic beam-

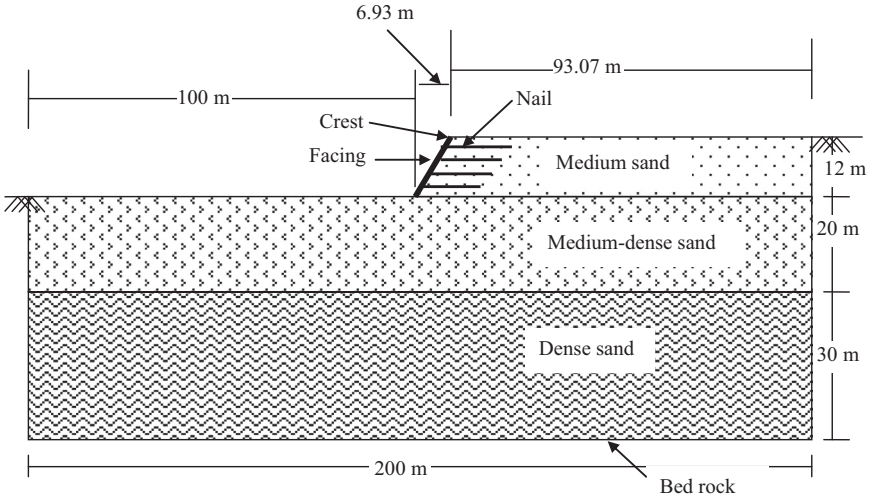

Fig. 1. Schematic of the model used in the present study.

Table 1
Details of nail used in analysis.

Item	
Total number of nails	5
Diameter (mm)	25
Length (m)	15
Horizontal spacing(m)	1
Vertical spacing(m)	2.4

column elements with three degrees of freedom, two translational and one rotational at each node.

3.2. Soil-nail interface

In reality, separation and sliding can take place at the soil-nail interface during earthquake shaking. In order to simulate such behavior, interface elements were introduced at the soil-nail interface. In addition to that, soil-nail interface was modeled as perfectly bonded, (i.e., no separation and sliding) to study the interface effects on the slope response. In the case of perfect contact, the soil nodes and the corresponding nail nodes (at the same location) were connected by equal degrees of freedom (DOF) constraint in both *x* and *y* directions. The nail

Table 2
Soil parameters used in the analysis.

Parameters	Layer 1	Layer 2	Layer 3
Soil type	Medium sand (Dr = 35%−65%)	Medium-dense sand (Dr = 65%−85%)	Dense sand (Dr = 85%−100%)
Unit weight (kN/m^3)	19	20	21
Poisson's ratio	0.33	0.35	0.35
Shear modulus (kPa)[a]	7.5×10^4	1.0×10^5	1.3×10^5
Bulk modulus (kPa)[a]	2.0×10^5	3.0×10^5	3.9×10^5
Friction angle (°)	33	37	40
Peak shear strain	0.1	0.1	0.1
Phase transformation (°) angle	27	27	27
contrac[b]	0.07	0.05	0.03
dilat1[c]	0.4	0.6	0.8
dilat2[d]	2	3	5

Note:
[a] At reference mean effective confining pressure of 80 kPa.
[b] *contrac* is a non-negative constant defining the rate of shearing induced volume contraction.
[c] *dilat1* and
[d] *dilat2* are non-negative constants defining the rate of shear induced volume increase.

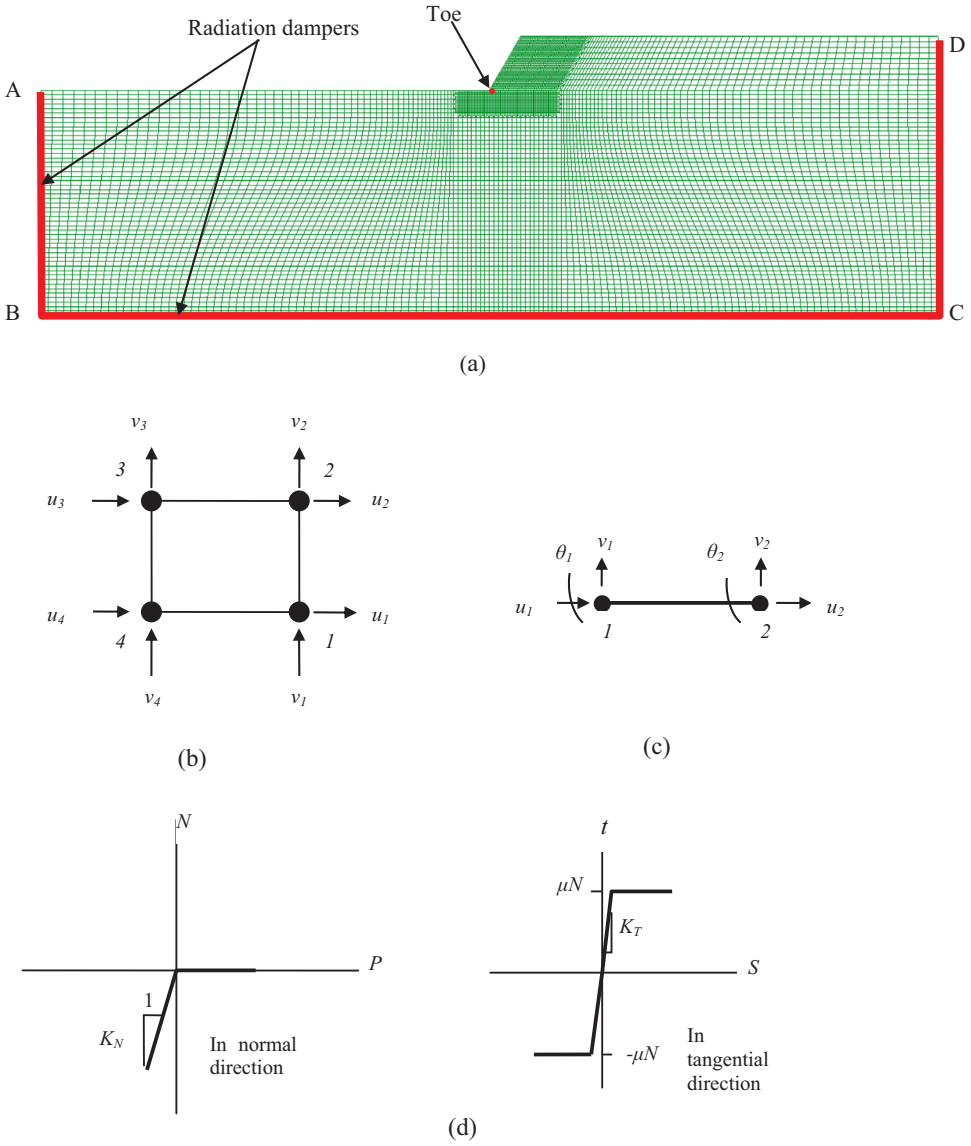

Fig. 2. Finite element model of the nailed soil slope: (a) soil-nailed slope model with element description; (b) area element for soil; (c) frame element for nail; (d) load-deformation relationships in soil-nail interface.

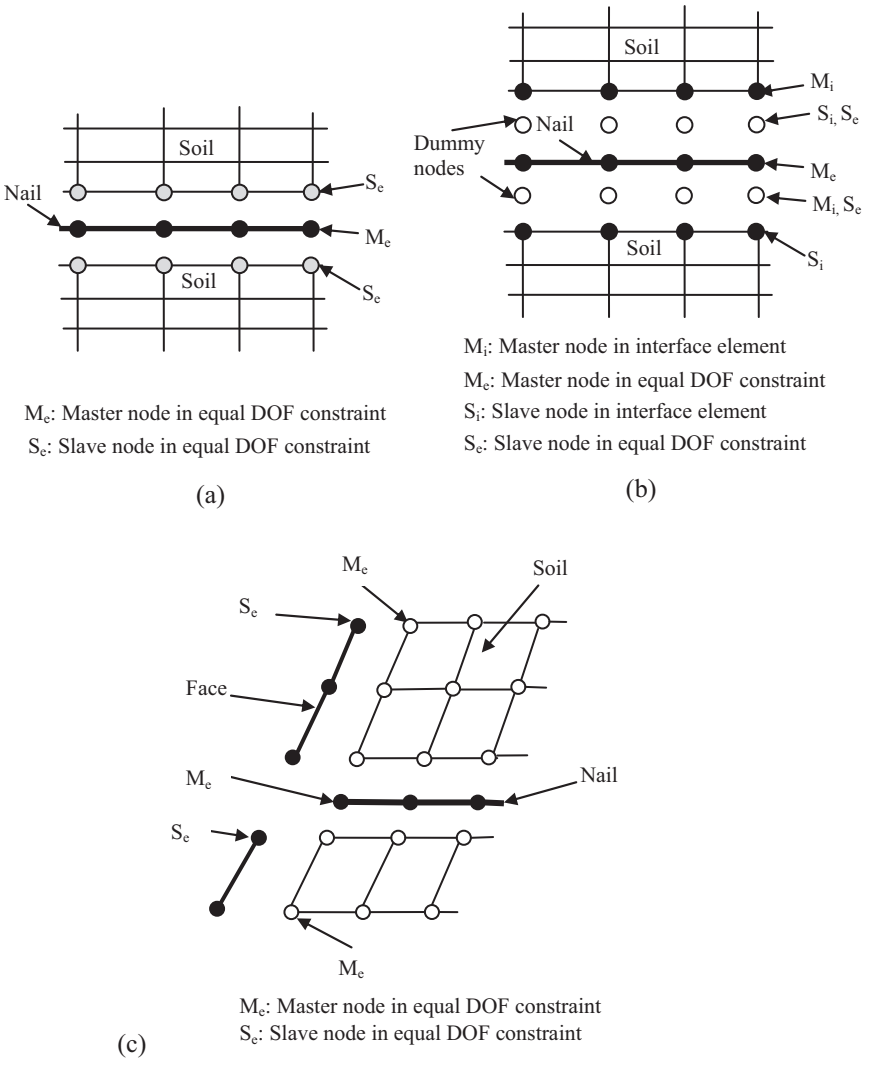

Fig. 3. Interface modelling (a) Soil-nail perfect bonding connectivity; (b) Soil-nail separation and sliding allowed (c) Facing-soil-nail connectivity.

Table 3
Parameters used in the analysis for interface elements.

Nail number[a]	K_N (kPa)	K_T (kPa)	μ[b]
1	7.80×10^4	1.56×10^4	0.4
2	1.35×10^5	2.70×10^4	0.4
3	1.74×10^5	3.48×10^4	0.4
4	2.06×10^5	4.12×10^4	0.4
5	2.34×10^5	4.68×10^4	0.4

Note: [a] nails have been numbered from top to bottom: [b] $\mu = \tan\left(\frac{2}{3}\phi\right)$.

nodes were treated as master nodes and corresponding soil nodes were treated as slave nodes, as shown in Fig. 3a.

For the case where separation and sliding were allowed, the soil-nail interfaces were modeled using node-to-node zero-length frictional contact elements available in OpenSees [8]. The formulation of these elements is based on penalty method. The zero-length frictional contact elements cannot be connected directly between the nail and soil element because these work only between the two nodes sharing the same space and with the same numbers of DOF [8]. The nodes of soil elements at the soil-nail interface had two DOF and the nodes of nails had three DOF. Therefore, a set of dummy nodes with two DOF each were introduced at all the interfaces as shown in Fig. 3b. The interface elements were connected between the soil nodes and the corresponding dummy nodes, and the dummy nodes were connected to the corresponding nail nodes using equal-DOF constraints in both the x and y directions. For proper simulation of the interface behavior, the master and slave nodes were identified while defining interface element as well as equal DOF constraints. The master and slave node assignment is depicted in Fig. 3b.

The interface element works on the Mohr-Coulomb friction law, expressed in terms of force, which is given as under:

$$T = C + \mu N \tag{2}$$

Where, T is the limiting tangential force at node, C is the total cohesion (summed over the tributary area for node, in present work it is zero), μ is friction coefficient at soil-nail interface and N is normal force at node. The sliding at soil-nail interface takes place when driving shear force t at a node reaches the limiting shear force T. The law simulates rigid-plastic sliding with no penetration. These constraints of no penetration and rigid-plastic sliding are enforced by penalty method. In penalty method, the constraints are fulfilled by defining certain stiffness in normal and tangential direction at contact surface between two bodies. When two bodies come in contact, normal stiffness (or stiffness coefficient, or normal penalty) K_N offers resistance to the penetration of one body into another. To have zero penetration, the value of K_N should be infinity. However, this causes numerical instability. Hence, to avoid numerical instability, certain finite but very large value of K_N is considered in the analysis which results into some (very small) penetration. The role of K_N in interface element has been depicted in Fig. 2d. Similarly, the constraint of rigid-plastic slip is fulfilled by tangential

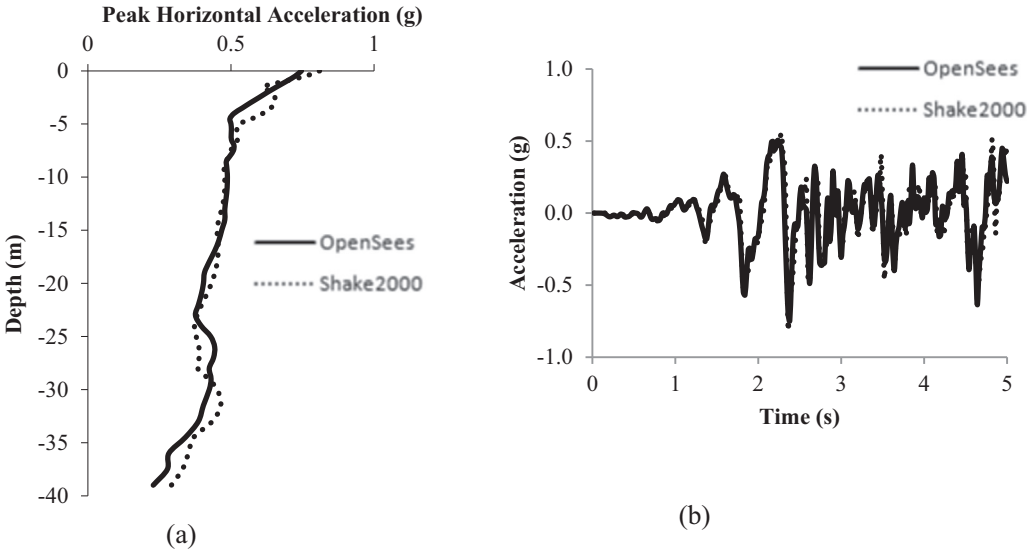

Fig. 4. Verification of OpenSees FE model with SHAKE2000 (a) Peak horizontal acceleration envelope; (b) Acceleration response history at ground surface.

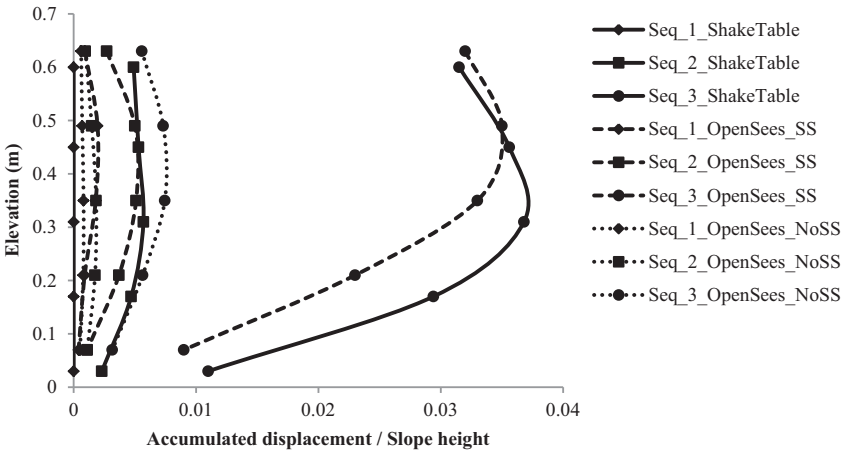

Fig. 5. Normalized accumulated facing displacement.

penalty K_T. Again, to have rigid-plastic slip, the value of K_T should be infinity. However, as mentioned above, this results in numerical instability. Hence, some finite but very large value of K_T is selected by allowing some (very small) sliding, prior to rigid-plastic slip, as shown in Fig. 2d. There is no hard and fast rule to select values of these coefficients. They depend on number of parameters such as geometry of problem, type of loading, materials in contact, etc. Hence, these values need to be obtained by iteration. In present study, to begin with, the stiffness of the soil (i.e., modulus of elasticity, E) at the depth where interface element is located has been taken as initial guess for both coefficients [23,24]. For the next iterations the value of K_T is kept constant and that of K_N is varied. This goes on until the penetration criterion is fulfilled. That is, the penetration at nodes reduces to the allowable penetration (in present case it is 0.5 mm). Next to this, iterations are carried out by keeping final value of K_N obtained in previous iteration constant and varying K_T until the convergence for sliding is achieved. In the present study, typically twenty iterations were carried out to obtain the acceptable values of K_N and K_T, which are listed in Table 3.

3.3. Facing-soil-nail connectivity

The face has also been modeled as elastic beam-column elements with three degrees of freedom as mentioned above. In the analysis, it is assumed that the nails are firmly fixed to the facing. The fixity between nails and facing has been modeled by defining equal degree of freedom constraints between nail nodes and the corresponding facing nodes in both x- and y-directions [25], as shown in Fig. 3c. The facing is assumed to be 300 mm thick (i.e., permanent facing of 200 mm and temporary facing of 100 mm) and having longitudinal and transverse reinforcement [26]. The modulus of elasticity for facing element is taken to be 2.24×10^7 kPa [27].

3.4. Boundary conditions and application of ground motion

The analysis has been carried out in four steps to properly imitate the in-situ condition of soil slope and to consider the radiation damping of soil properly. In the first step, gravity analysis was carried out for the self-weight of the soil-nail model to develop the desired confining pressure to all the soil elements. In this step, the soil was assumed to behave as linear elastic material and the side boundaries (AB and CD in Fig. 2a) of the soil-nail model were horizontally restrained and vertically free, whereas base boundary (BC in Fig. 2a) was fixed in both the directions. With these boundary conditions, the soil constitutive model was switched from linear-elastic to elasto-plastic, and then equilibrium state under gravity was obtained iteratively. The reaction forces at the boundary nodes were obtained at the end of this step. In the third step, these reaction forces were statically applied at the respective boundary nodes, and the boundary restraints were removed completely. This state of the model was assumed as the initial condition of the soil-nail system for seismic analysis. In the final step, Lysmer-Kuhlemeyer's [9] radiation dampers were added at the boundary nodes, and the earthquake motion was applied at the base nodes(BC in Fig. 2a) as equivalent nodal shear force proportional to the velocity of incident seismic wave by

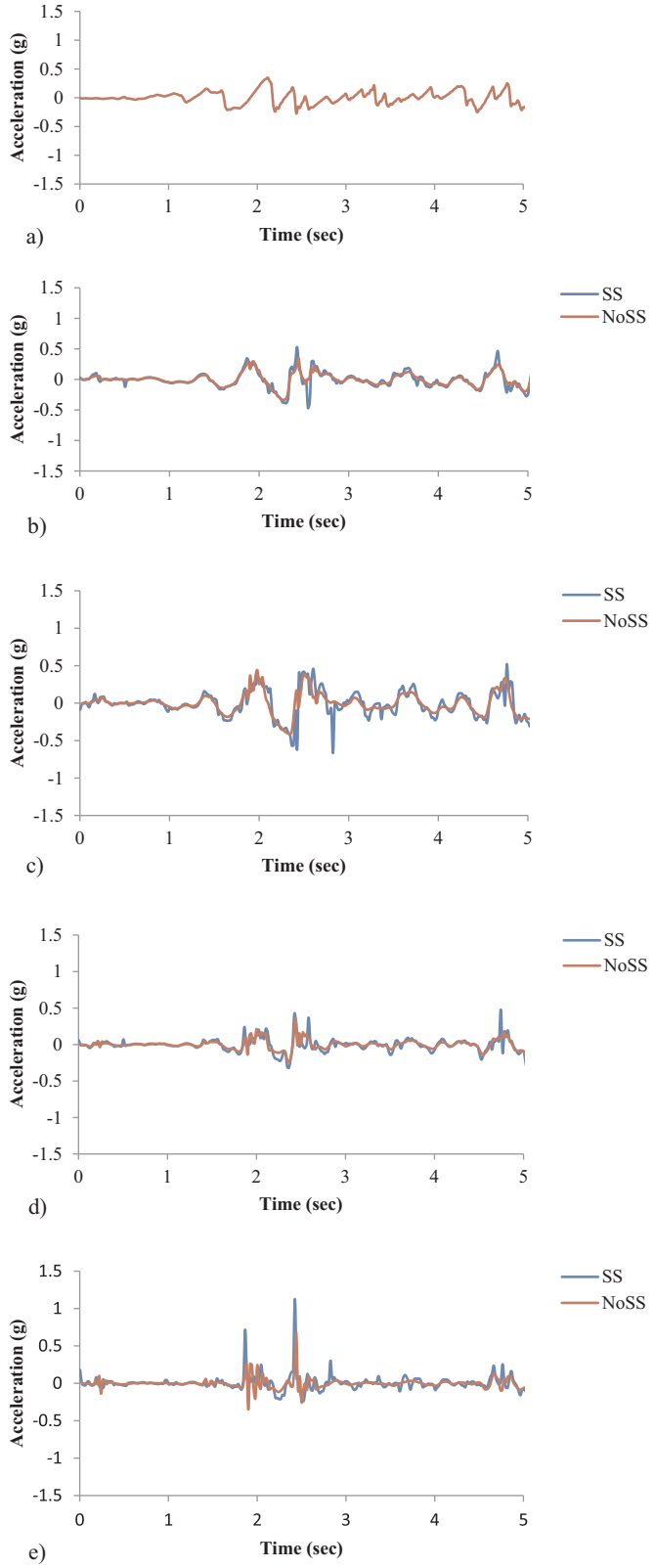

Fig. 6. Acceleration records: (a) Input acceleration-time history (b) Horizontal accelerations at Toe; (c) Horizontal accelerations at Crest; (d) Vertical accelerations at Toe; (e) Vertical accelerations at Crest.

following the method proposed by Joyner and Chen [28]. The radiation dampers were zero-length elements with two nodes; one node was connected to the boundary soil node and the other node was fixed in space. The coefficients of the horizontal and vertical dampers at the side boundaries were estimated as $\rho v_p A$ and $\rho v_s A$, where, ρ, v_s, v_p are, respectively, the mass density, shear wave velocity and longitudinal wave velocity of soil outside the computational domain, and A is the tributary area of the node. Similarly, the coefficients of the horizontal and vertical dampers at the base boundaries were estimated as $\rho v_s A$ and $\rho v_p A$.

4. Verification and validation

OpenSees finite element analysis (FEA) has been verified with equivalent 1-D linear analysis using commercial software SHAKE2000 [29]. For verification purpose, free field analyses have been carried out in both OpenSees and SHAKE2000. The motion was applied at the base in both models. The objective was to verify the effectiveness of radiation boundaries and the mesh size considered in OpenSees model and the time step considered for the analysis. The soil was assumed to behave as linear-elastic material in both OpenSees and SHAKE2000. The north-south component of horizontal acceleration (PGA = 0.348 g) recorded at El-Centro during 1940 Imperial Valley earthquake was used as input motion for the verification. Peak horizontal acceleration profile across the depth obtained from both of the models has been compared in Fig. 4a, which shows good agreement. Acceleration response histories obtained from OpenSees and SHAKE2000 analyses for a node at ground surface are also compared in Fig. 4b. Fig. 4 shows that there is good agreement between OpenSees and SHAKE2000 results.

In addition to this, validation of the OpenSees finite element analysis (FEA) has been done with the results of the shaking table tests on cohesionless soil conducted by Hong et al. [30]. They conducted a series of tests on 80° and 90° nailed slopes of height 0.7 m. For the validation purpose, 90° slope with horizontal nails of length 0.4 m has been considered. The relative density of the sand used in the Shaking Table test was 61.8%, which corresponds to the medium dense sand. The shear modulus and bulk modulus used in FEA are calculated from the dynamic modulus of elasticity given in the article. Other constitutive parameters have been taken from OpenSees reference manual corresponding to medium sand. The geometry of domain and the properties of nails and facing are kept the same as in shaking table test. The earthquake motion considered in both shaking table test and FEA is the east-west component of 1999 Chi-Chi Earthquake at observatory station TCU 074. In FEA the earthquake motion is applied at the base nodes as uniform excitation to simulate the mode of application of motion in shaking table test. Normal and tangential dashpots are provided at the side boundaries of the model to take care of radiation damping. To compute the dashpot coefficients shear modulus, density and Poisson ratio of mild steel, which represents the sidewall material of container in shaking table test, has been considered (i.e., $G = 7.8 \times 10^7$ kPa, $\rho = 78$ kN/m^3, $\mu = 0.3$). The motion has been applied as mentioned by by Hong et al. [30]. The plots of normalized facing displacement (by height of slope) obtained from FEA have been compared with those from shaking table test as shown in Fig. 5. Elevations in FEA plots correspond to nail head positions, which are close to those considered in the test. Two cases of soil-nail interface modelling considered in the present study are: no separation and sliding (NoSS) between nail and soil and; allowing the separation and sliding (SS) between nail and soil. It is observed from Fig. 5 that the normalized facing displacements in NoSS case are much smaller than those in shaking table test. Comparison of plots at the end of third sequence shows that the normalized displacements in NoSS case are about 71–82% smaller than those from shaking table test. On the other hand, the facing displacements in SS case are just 2–22% smaller than those in shaking table test. In addition to this, the peak normalized displacement in SS case is just 5% smaller than that in test. This implies that modelling of soil-nail interface in FEA as perfectly bonded significantly underestimates the deformation. The discrepancy in the shaking table test plots and SS plots could be attributed to the relatively crude selection of the material parameters for sand in FE simulation due to their unavailability in the article by

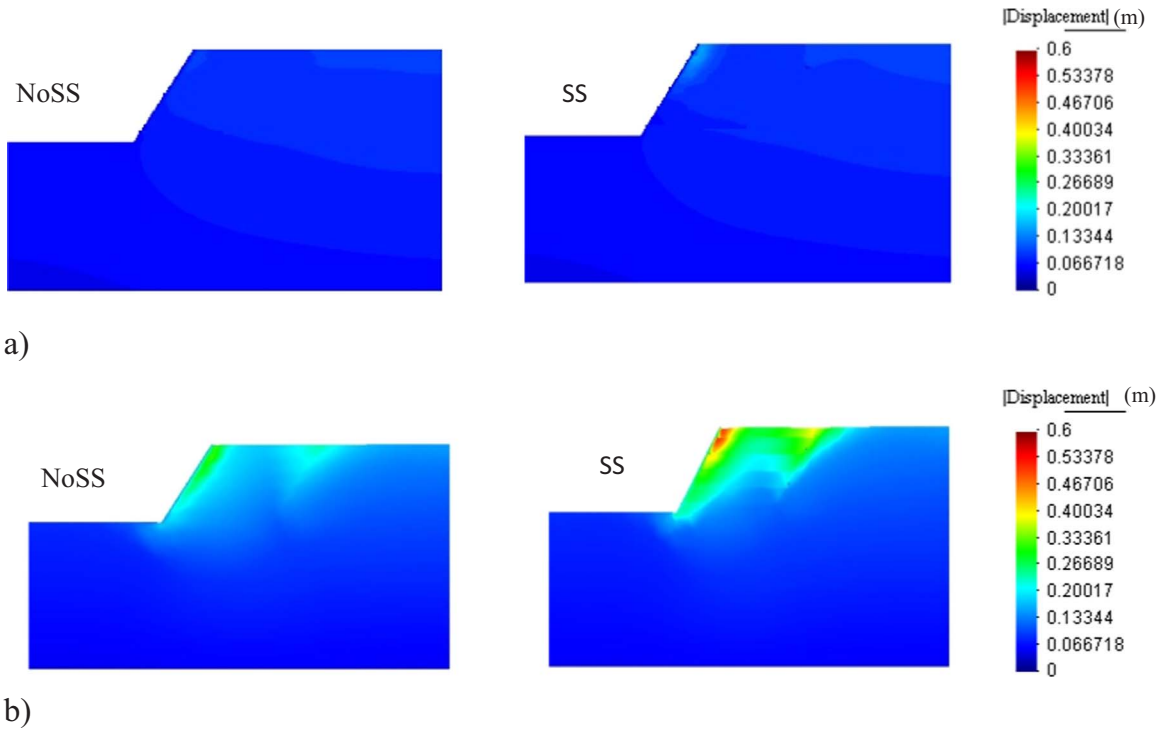

Fig. 7. Deformation contours: (a) NoSS and SS at 2.12 s; (b) NoSS and SS at 53.74 s.

Hong et al. [30]. In addition, there could be some difference, though only a little, in the energy absorption and reflection at the side boundaries in FEA and shaking table test. Taking into account above constraints it can be concluded that the results obtained from OpenSees simulation for SS case are acceptable.

5. Overall deformation and failure pattern considering interface effect

The seismic FE analyses have been carried out for nailed slope with two different conditions of soil-nail interface, NoSS and SS. The slope considered in the analysis has inclination of 60° and it is analyzed for the south-east component of 1940 Imperial Valley earthquake (M 6.9) motion. The input motion has duration of 53.74 s and Peak Ground Acceleration (PGA) of 0.348 g. A part of input acceleration record is shown in Fig. 6. The input motion has been applied at nodes at the base of the model.

5.1. Acceleration amplification

In reality, the frequencies ranging from 0.1 to 25 Hz are of interest as they only contribute to the seismic response of structure [28]. However, in case of finite element analysis higher modes of frequencies get induced into the analysis as a part of discretization. i.e., these higher modes of frequencies are just artificial [31,32]. These artificial higher modes of frequencies severely affect the acceleration response of the system. However, their effect on displacement response is negligible [31]. Hence, to get the correct acceleration response the frequencies higher than 25 Hz need to be damped out. In the present study, this has been achieved by using Newmark Integration Method and selecting the corresponding parameters as per the “unconditionally stable” criterion [32].

The PGA for the input motion occurs at 2.12 s. The seismic response of the nailed slope can be significant around this time. Hence, acceleration time records at Toe and Crest have been considered and compared for a time span up to 5 s for both NoSS and SS case, as shown in Fig. 6. From this figure, it is clear that both horizontal and vertical acceleration reach their maximum value at around 2.4 s, as expected in both cases. In NoSS case, absolute maximum horizontal acceleration at Toe and Crest is 0.35 g and 0.34 g, respectively, indicating that amplification factor is around 1. However, in SS case, the absolute maximum horizontal acceleration at Toe and Crest is 0.53 g and 0.67 g, respectively. This shows that the corresponding amplification factors are 1.52 and 1.91, respectively. In NoSS case, the maximum vertical acceleration at Toe and Crest is 0.35 g and 0.68 g, respectively. Whereas, the maximum vertical acceleration at Toe and Crest is 0.48 g and 1.13 g, respectively, in SS case. From above discussion it is clear that amplification is more in SS case. In addition to this, the amplification factors for vertical acceleration at Crest are larger than rest of all. This is so because when vertically propagating shear wave reaches Toe of slope, facing experiences horizontal jerk at the Toe. This jerk causes both outward and downward movement of the upper part of facing. It is similar to a ladder resting against a wall and moved at base horizontally. In this case, the top of ladder moves both downward and outward even though base is moved horizontally only. Same physics follows in case of facing in present study. This phenomenon continues as wave propagates upward. Anchorage effect of nails prevents lateral displacement of facing. However, contribution of nails to prevent vertical movement of facing is small. It means that facing is relatively free to move in vertical direction. This freedom is more at the top part of facing. Owing to all above mentioned reasons, though applied input motion is horizontal, facing experiences big vertical movement, and results into high vertical accelerations at Crest This implies that the vertical acceleration should also be given due importance in stability analysis of such slopes.

5.2. Overall deformation

To study the overall deformation of slope, the deformation contours have been shown in Fig. 7 at two time steps 2.12 s and 53.74 s. The deformations at these times have been considered because the input motion had peak acceleration at 2.12 s and the total duration of input motion was 53.74 s. The deformation is considered significant at 2.12 s and permanent deformation is expected to occur at 53.74 s. From Fig. 7,

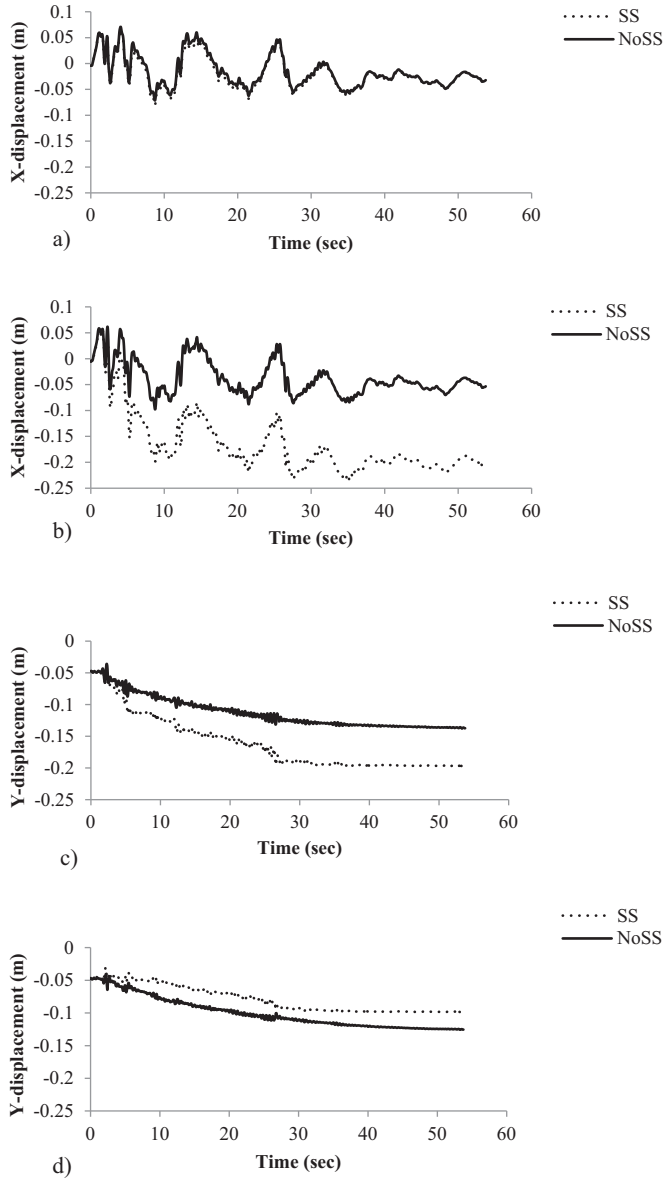

Fig. 8. Toe and Crest displacements: (a) Horizontal (i.e., X) displacements at Toe; (b) Horizontal (i.e., X) displacements at Crest; (c) Vertical (i.e., Y) displacements at Toe; (d) Vertical (i.e., Y) displacements at Crest.

Table 4
Displacements at Toe and Crest at the end of seismic shaking.

Displacement component	NoSS	SS
Horizontal displacement at toe (m)	0.032	0.033
Vertical displacement at toe (m)	0.137	0.197
Horizontal displacement at crest (m)	0.053	0.204
Vertical displacement at crest (m)	0.125	0.098

it is clear that the deformation is much smaller in case of NoSS compared to SS case. The value of maximum displacement at 2.12 s is found to be 0.10 m and 0.17 m for NoSS and SS case, respectively. Whereas at the end of seismic shaking, i.e., at 53.74 s, the maximum displacement is found to be 0.60 m and 0.27 m for SS and NoSS case, respectively. It means that the maximum displacement in case of SS case is about 2.25 times greater than that in case of NoSS. In NoSS case, the deformation is mainly observed in a local region near the facing. This could be attributed to the increase in the stiffness of reinforced soil mass due to the large interface strength artificially induced by the perfect bonding between soil and nail.

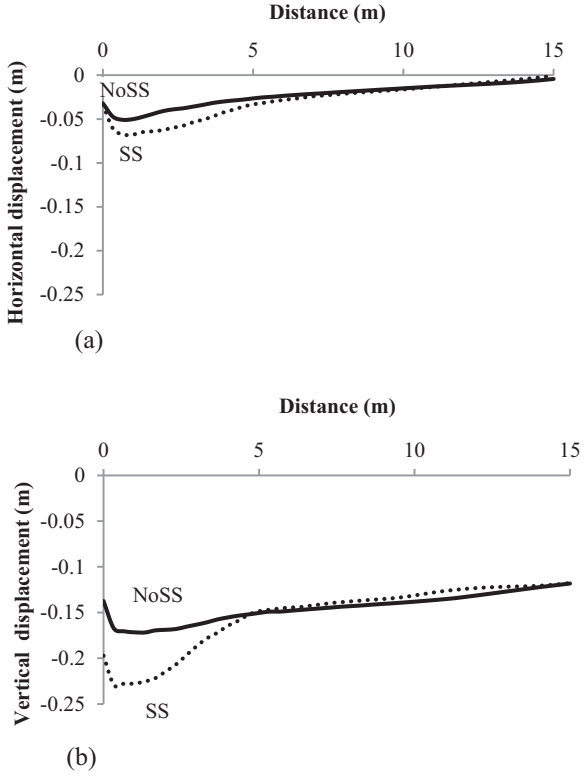

Fig. 9. Displacements at the base of slope: a) Horizontal displacements; b) Vertical displacements.

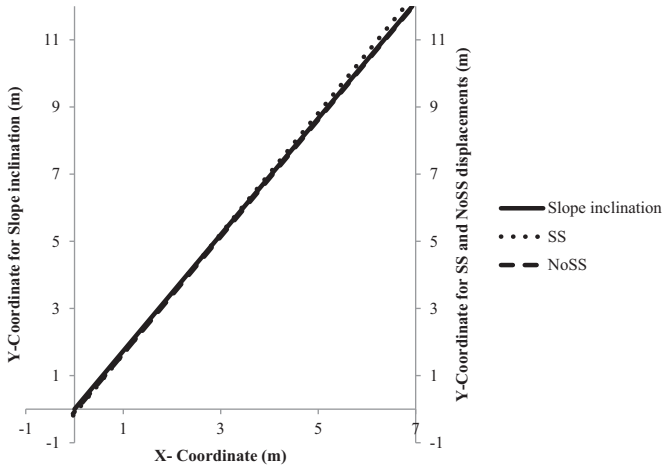

Fig. 10. Facing displacements at the end of seismic shaking for SS and NoSS case.

5.3. Toe and Crest displacements

The variation of horizontal and vertical displacements, during shaking, at the Toe and Crest of slope has been shown in Fig. 8. The displacements at the end of seismic shaking are given in Table 4. Fig. 8a indicates that the horizontal displacement at Toe is almost same in both NoSS and SS cases. This is attributed to the significant resistance offered by facing to the horizontal movement at toe in both NoSS and SS case. This can be justified with the help of Fig. 9a which gives the horizontal displacement along the base of slope (i.e., along a horizontal plane passing through toe) at the end of seismic shaking. In addition to this, Fig. 9a shows that at a distance of 0.66 m behind the toe the horizontal displacement in case of SS is about 1.3 times that in NoSS case. This

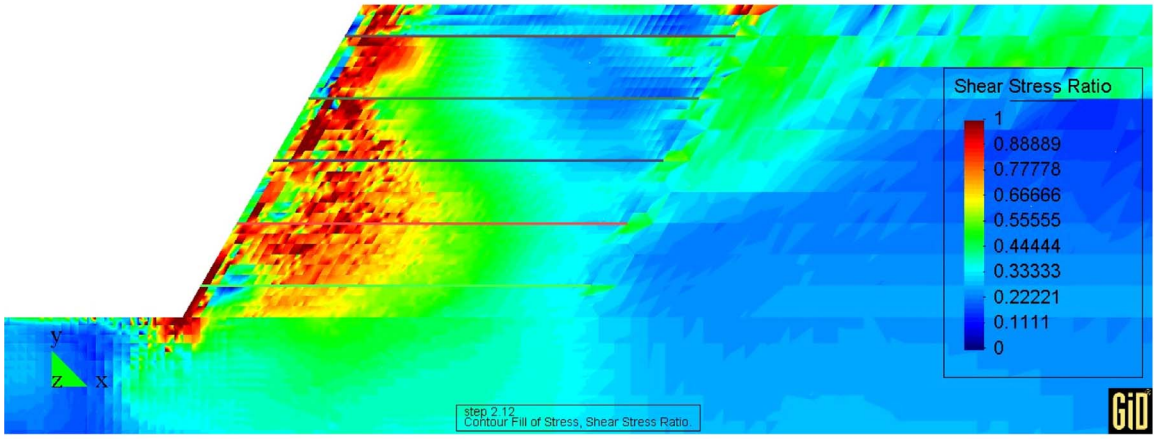

a) NoSS

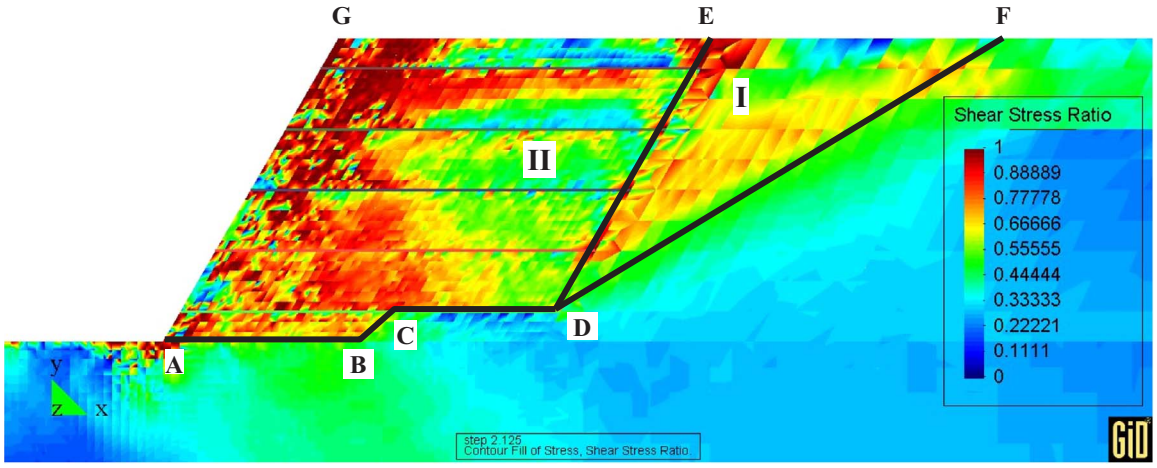

b) SS

Fig. 11. Shear stress ratios for NoSS and SS at 2.12 s.

difference goes on reducing and becomes zero at a distance of about 11 m. Beyond this distance the horizontal displacement is more or less same in both cases. This implies that the interface modelling has significant effect on the horizontal displacement along the base except at the toe. From Table 4 it is clear that the vertical toe displacement in SS case is 1.4 times that in NoSS case. The variation in vertical displacement behind the toe is much smaller in NoSS case than in SS case, as shown in Fig. 9b, implying that the reinforced soil mass behaves more like a rigid block in NoSS case. A sudden increase in the vertical displacement, behind toe up to a distance of 5 m, is observed in SS case implying relatively flexible behavior of reinforced soil mass in this case. From Table 4 it is clear that the horizontal displacement of crest in SS case is about 4 times that in NoSS case. This is mainly because of the sliding of soil mass at soil-nail interface in SS case, which keeps the simulated soil mass relatively flexible and deformable. However, the vertical displacement of crest for SS case is about 0.8 times that in NoSS case. This is due to significantly larger horizontal movement at crest, in SS case, which in turn suppresses vertical movement to some extent.

5.4. Facing displacement

Fig. 10 shows the displacement of facing at the end of seismic shaking for both SS and NoSS case. Both the plots are observed to be straight. It means that the facing has displaced but not deformed, during shaking. This could be attributed to relatively stronger facing considered in the present analysis. In reality, as well, facing is about 300 mm thick (i.e., permanent facing of 200 mm and temporary facing of 100 mm) and having longitudinal and transverse reinforcement [26] which in turn makes it stronger. From Fig. 10, it is clear that the displacement of facing is significant when separation and sliding is allowed at soil-nail interface. Horizontal displacement is found to be significant at top whereas vertical displacement is observed to be significant at bottom (i.e., a kind of sinking). This type of sinking of facing bottom was also observed during centrifuge testing of nailed slopes conducted by Tufenkjian and Vucetic [33]. The overburden pressure on the topmost nail is small due to which larger horizontal displacement of facing takes place. Moving down towards the bottom of facing the overburden pressure on the nail increases significantly, this in turn reduces horizontal displacement of facing. The displacement of facing is found to be very small when there is perfect bonding between soil and nail. Owing to this, the displacement plot for NoSS case is as if it coincides with the initial position of facing.

5.5. Nature of failure pattern in terms of shear stress ratio (SSR)

Shear stress ratio is defined as the ratio of shear stress to the peak

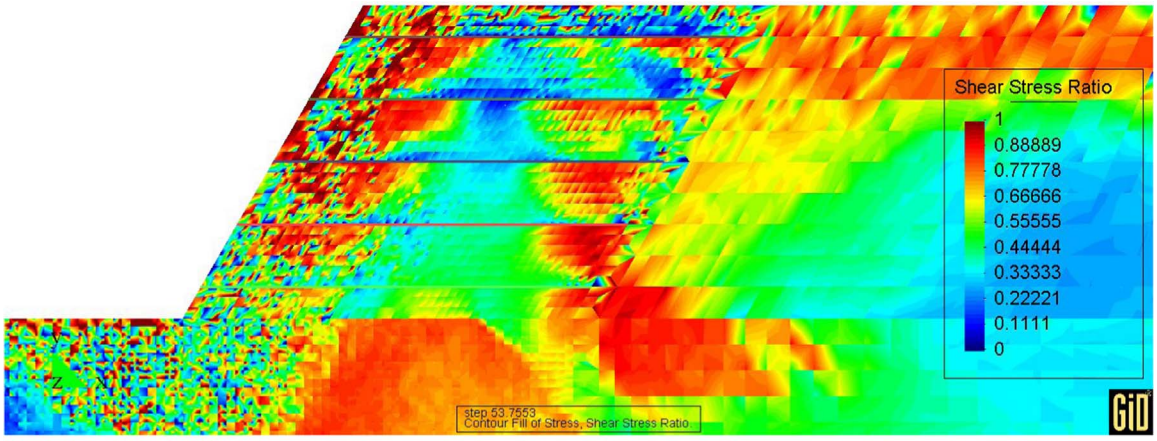

a) NoSS

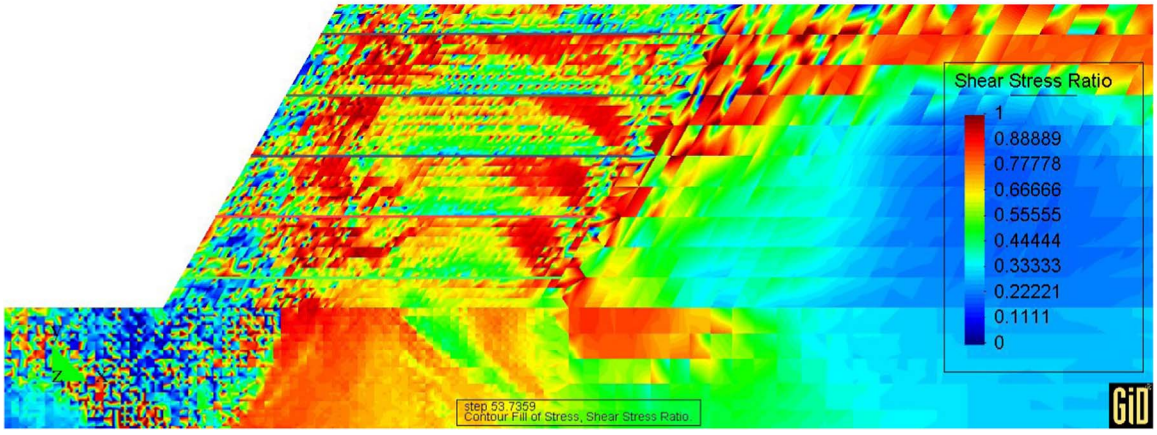

b) SS

Fig. 12. Shear stress ratios for NoSS and SS at 53.74 s.

shear strength at the current confining pressure. It varies between 0 and 1. When its value becomes 1, it means that the full peak shear strength is mobilized and material can be assumed to have failed in shear. Contours for the SSR values in the model domain have been shown in Figs. 11 and 12 for both types of interfaces to understand the degree of shear strength mobilized. SSR is considered at time 2.12 s in Fig. 11 and at 53.74 s in Fig. 12, respectively. At 2.12 s shear strength is fully mobilized only in the vicinity of facing, in NoSS case, as shown in Fig. 11a. Further, in NoSS case the zone of shear strength mobilization becomes broad at nail-3 and nail-4. In the region of nail heads, the SSR varies from 0 to 0.47, for NoSS case, implying that the soil mass in this region has reserved strength. From Fig. 11b it is observed that in SS case, the SSR is above 0.5 for most of the reinforced soil mass and is equal to 1 along the slope facing. In addition to this, in the region of nail tails the SSR ranges from 0.70 to 1 implying that there could be subsidence of soil mass in this region. In NoSS case, the zone in which SSR is about 1 gets reduced in size and is shifted towards the facing of slope. It means that failure zone shifted from global to local and involved less soil mass. Being perfectly bonded the stiffness of the nails contributes to the overall stiffness of the soil surrounding it, which in turn results into increase in the apparent shear strength of the soil in the vicinity of nail. Fig. 12a shows that the shear strength has been mobilized in the area comprising about one-third nail length from the facing of slope in NoSS case. In addition to this, in the vicinity of the tails of the third and fourth nails SSR is observed to be 1. SSR around the bottommost nail except at its tail is less than 1 in NoSS case. In SS case, the shear strength is mobilized all along the nail length except in the close vicinity of facing as observed in Fig. 12b.

For some region below the nailed soil mass, SSR is observed to be 1 at 53. 74 s, implying the local failure (i.e., small compression) of soil mass in this region. As the nailed soil mass behaves monolithically, during shaking vertical component of inertial force of this mass will try to compress the subsoil cyclically. Owing to this, subsoil will have local failure (i.e., small compression). This can be justified from comparison of shear stress ratios at 2.12 s and 53.74 s.

5.6. *Two wedge failure mechanism*

A two wedge failure mechanism, wedge I and wedge II, as shown in Fig. 11 b is observed in the present study. The failure surface DE is parallel to the facing Hong et al. [30] performed a series of shaking table tests on nailed soil slopes and found a similar failure surface. A failure zone encompassed by wedge I was observed during the experimental study conducted by other researchers [33,30]. The failure surface ABCD observed in present study is a little different from that observed by Tufenkjian and Vucetic [33] and Hong et al. [30]. They observed a straight failure surface AD emerging at toe and passing though bottom nail(s) without a discontinuity surface BC as observed in present study. In present work, nails are relatively long (L/H = 1.25). Owing to this, whole nailed soil mass behaves as a single unit and slides

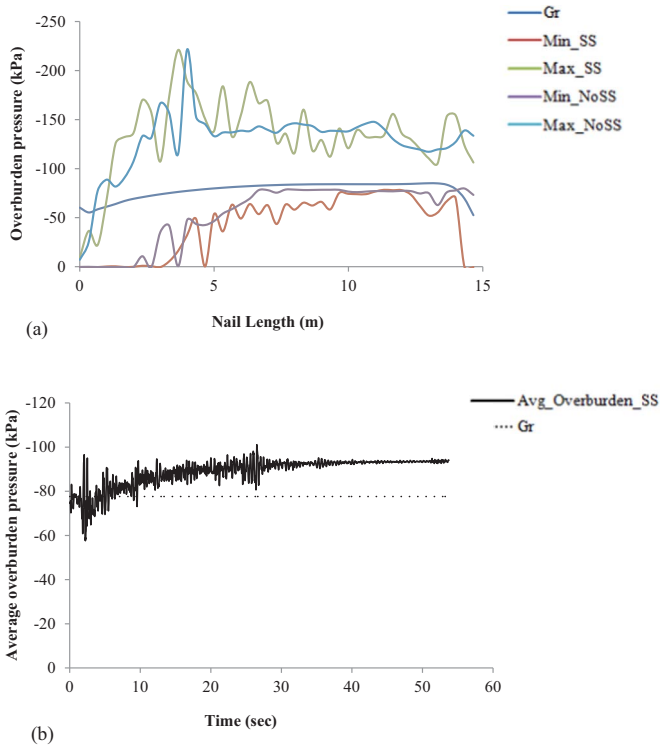

Fig. 13. Overburden pressure envelopes: (a) Maximum and Minimum Overburden pressure envelopes for Nail-3; (b) Average overburden pressure envelope for Nail-3.

on the bottom nail. This might be the reason, due to which failure surface at the bottom have not been developed through nails.

In conventional pseudo-static analysis of nailed slopes, bi-linear failure surface is assumed, i.e., German method [34,35,36]; CALTRANS (computer program SNAIL [37]) etc. Out of these two methods German method assumes a failure surface similar to DE and parallel to facing. In CALTRANS failure surface is assumed similar to ADF (with no discontinuity BC). Present analysis supports the failure surface assumed in the German method more closely than that assumed in CALTRANS.

6. Effect of interface modelling on variation of overburden pressure

During stability analysis of nailed soil slopes, the value of overburden pressure along the nail length is to be known to determine the pull-out capacity of nails. In pseudo-static method of analysis, the overburden pressure on the nail is generally assumed to be constant [38]. However, for the seismic condition such assumption may or may not be valid because the vertical stress at any point in the soil mass can vary during seismic shaking. Therefore, the effect of seismic shaking on the vertical stress along the nail length has been analyzed for the same model of soil-nail system.

As the shaking goes on, the overburden pressure at each node may vary. It can either increase above the gravity overburden pressure or decrease below it due to vertical acceleration components. Thus, each node will have a maximum and a minimum value of overburden pressure over the duration of shaking. The maximum and minimum overburden pressure envelopes for both NoSS and SS cases for the third nail (Nail-3) have been plotted in Fig. 13a as a typical case and compared with gravity overburden pressure envelope (*Gr*). The maximum and minimum overburden pressure envelopes are the locus of maximum and minimum overburden pressure values, respectively, at each node along nail length. There are total five nails in the model and have been numbered from top to bottom. Thus, Nail-3 is at the mid height of the slope. Similar comparison was made for remaining four nails as well. As expected the Maximum and Minimum overburden pressure envelopes were on higher and lower side of the gravity overburden pressure (*Gr*) envelope, respectively. The fluctuation in overburden pressure along the nail length was found to be more in case of SS than that in case of NoSS. This can be attributed to the relatively large movement of soil mass in case of SS owing to the sliding and separation at the soil-nail interface. In addition to this, the fluctuation is more at the facing, probably because of the large movement of soil mass due to less confinement there. Moving away from the facing the confinement becomes significant, because of which the fluctuation in the overburden pressure reduces. From Fig. 13a it is observed that beyond a distance of about 7 m from the facing, the Minimum overburden pressure envelopes for both cases move closer to the gravity overburden pressure envelope. This will help to increase the pull-out capacity of the nail. Near the facing, the minimum overburden pressure is found to be zero. This is attributed to the loosening and failure of the soil mass around the nail in this region.

The time variation of the average overburden pressure over the nail length has been compared with the gravity overburden pressure (*Gr*) in Fig. 13b. Significant reduction in the average overburden pressure around the nails for a short duration can lead to large displacement of facing-nail system, i.e., the facing-nail system may experience large outward movement. For all the nails the average overburden pressure exceeds the gravity overburden pressure, except for a small duration in early part of loading. The decrease in average overburden pressure below gravity overburden pressure results into a small outward movement of facing-nail system. This outward displacement of facing-nail system is observed in Fig. 10.

The authors' feel that the SS represents more realistic behavior of nailed soil slopes and hence, the results obtained from the same should be used as basis for the stability analysis of nailed soil slopes subjected to earthquake loading. Pseudo-static method is a widely used method for seismic stability analysis of reinforced slopes. In this method the overburden pressure on the nail is assumed to be constant and equal to the gravity overburden pressure. With the help of Fig. 13, it can be said that this assumption may lead to a relatively conservative design, but it is acceptable from practical point of view. In the present study only horizontal motion was considered. If vertical motion is also incorporated the situation may be different.

7. Conclusions

The soil-nail interface modelling is found to play important role in displacement based analysis of nailed soil slope. It is observed that the deformation of slope is significantly more when sliding and separation is allowed. The displacement of facing is observed to be significant at the top in SS case whereas it is very small in NoSS case. By referring to the experimental studies carried out in past by other researchers and findings in the present study; it can be said that the NoSS case fails to simulate the facing displacement. In addition to this, the failure surface observed in the present study is close to the bi-linear failure surface assumed in the German method. Hence, authors recommend use of the German method in the pseudo-static analysis of nailed soil slopes. It is found that vertical acceleration at toe as well as crest is significantly large. Hence, it should be given due weightage in pseudo static analysis by selecting appropriate vertical seismic coefficient. Overburden pressure on the nail is found to have large variation during the shaking. Again this variation is more in case of SS. The performed analysis based on horizontal seismic excitation indicates that in pseudo-static method the overburden pressure on the nail can be conveniently assumed equal to the gravity overburden pressure although it is a relatively conservative.

References

[1] Vucetic M, Tufenkjian MR, Felio GY, Barar P, Chapman K. Analysis of soil-nailed excavations stability during the 1989 Loma Prieta earthquake. USGS Professional

Paper 1552-D: The Loma Prieta, California, Ee4dsarthquake of October 17, 1989 Perfomace of the Built Environment—Earth Structures and Engineering Characterization of Ground Motion; 1998. p. D27-D45.
[2] Griffiths D, Lane P. Slope stability analysis by finite elements. Geotechnique 1999;49(3):387–403.
[3] Zhang M, Song E, Chen Z. Ground movement analysis of soil nailing construction by three-dimensional (3-D) finite element modeling (FEM). Comput Geotech 1999;25(4):191–204.
[4] Wang Z, Richwien W. A study of soil-reinforcement interface friction. J Geotech Geoenviron Eng 2002;128(1):92–4.
[5] Ann TS, Cheang W, Hai OP, Tan D. Finite element analysis of a soil nailed slope-some recent experience. In: Proceedings of the 3rd Asian regional conference on geosynthetics: now and future of geosynthetics in civil engineering, Seoul, Korea; 2004.
[6] Fan CC, Luo JH. Numerical study on the optimum layout of soil–nailed slopes. Comput Geotech 2008;35(4):585–99.
[7] Sahoo S, Manna B, Sharma KG. Stability analysis of steep nailed slopes underseismic condition using 3-D finite elementmethod. Int J Geotech Eng 2015;9(5):536–40.
[8] Mazzoni S, McKenna F, Scott MH, Fenves GL. OpenSees command language manual. Pacific Earthquake Engineering Research (PEER)Center; 2006.
[9] Lysmer J, Kuhlemeyer RL. Finite dynamic model for infinite media. J Eng Mech Div, ASCE 1969;95(4):859–77.
[10] Michalowski RL. Soil reinforcement for seismic design of geotechnical structures. Comput Geotech 1998;23(1):1–17.
[11] Michalowski RL, You L. Displacements of reinforced slopes subjected to seismic loads. J Geotech Geoenviron Eng 2000;126(8):685–94.
[12] Iwan WD. On a class of models for the yielding behavior of continuous and composite systems. J Appl Mech 1967;34(3):612–7.
[13] Mroz Z. On the description of anisotropic workhardening. J Mech Phys Solids 1967;15(3):163–75.
[14] Prevost JH. A simple plasticity theory for frictional cohesionless soils. Int J Soil Dyn Earthq Eng 1985;4(1):9–17.
[15] Parra-Colmenares EJ. Numerical modeling of liquefaction and lateral ground deformation including cyclic mobility and dilation response in soil systems Ph.D. Thesis Troy, N.Y: Dept. of Civil Engineering, Rensselaer Polytechnic Inst.; 1996.
[16] Yang Z. Numerical modeling of earthquake site response including dilation and liquefaction [Ph.D. Thesis]. New York: Dept. of Civil Engineering and Engineering Mechanics, Coulombia University; 2000.
[17] Elgamal A, Yang Z, Parra E, Ragheb A. Modeling of cyclic mobility in saturated cohesionless soils. Int J Plast 2003;19(6):883–905.
[18] Yang Z, Elgamal A, Parra E. Computational model for cyclic mobility and associated shear deformation. J Geotech Geoenviron Eng 2003;129(12):1119–27.
[19] Yang Z, Lu J, Elgamal A. OpenSees soil models and solid-fluid fully coupled elements user manual. San Diego: Univ. of California; 2008〈http://cyclic.ucsd.edu/opensees/〉.
[20] Kuhlemeyer RL, Lysmer J. Finite element method accuracy for wave propagation problems. J Soil Mech Found Div 1973;99(SM5):421–7.
[21] Al-Hussaini MM, Johnson LD. Numerical analysis of a reinforced earth wall. In: Proceedings, symposium on earth reinforcement, ASCE, Pittsburg; 1978 p. 98-126.
[22] Hsien LC. Finite element study of 2D equivalence to 3D analysis of a discrete soil nail problem with applications to serviceability design [M.E. thesis]. National University of Singapore; 2003.
[23] Kolay C. Seismic analysis of bridge abutment-soil systems. India: Master of technology project report, Indian Institute of Technology Kanpur; 2009.
[24] Mondal G, Prashant A, Jain SK. Significance of interface nonlinearity on the seismic response of a well-pier system in cohesionless Soil. Earthq Spectra 2012;28(3):1117–45.
[25] Zhou YD, Cheuk CY, Tham LG. Numerical modelling of soil nails in loose fill slope under surcharge loading. Comput Geotech 2009;36(5):837–50.
[26] Lazarte CA, Robinson H, Gómez JE, Baxter A, Cadden A, Berg R. Soil Nail Walls Ref Man 2015. [No. FHWA-NHI-14-007].
[27] Kulkarni SK, Shiyekar MR, Shiyekar SM, Wagh B. Elastic properties of RCC under flexural loading-experimental and analytical approach. Sadhana 2014;39(3):677–97.
[28] Joyner WB, Chen AT. Calculation of nonlinear ground response in earthquakes. Bull Seismol Soc Am 1975;65(5):1315–36.
[29] Ordonez G. SHAKE2000–A computer program for the 1-D analysis of geotechnical earthquake engineering problems. Lacey, Washington, USA: User's Manual, GeoMotions, LLC; 2005. p. 358.
[30] Hong YS, Chen RH, Wu CS, Chen JR. Shaking table tests and stability analysis of steep nailed slopes. Can Geotech J 2005;42(5):1264–79.
[31] Broderick BM, Elnashai AS, Izzuddin BA. Observations on the effect of numerical dissipation on the nonlinear dynamic response of structural systems. Eng Struct 1994;16(1):51–62.
[32] Hughes TJ. The finite element method: linear static and dynamic finite element analysis. Cour Corp 2012.
[33] Tufenkjian MR, Vucetic M. Dynamic failure mechanism of soil-nailed excavation models in centrifuge. J Geotech Geoenviron Eng 2000;126(3):227–35.
[34] Gassler G, Gudehus G. Soil nailing-some aspects of new technique. In: Proceedings of the 10th International Conference on Soil Mechanics and Foundation Engineering: Balkema, Rotterdam, V. 3; 1981. p. 665–70.
[35] Lambe PC, Jayaratne NN. Construction of retaining walls from the top down: center for transportation engineering studies, department of civil engineering. North Carolina State University at Raleigh; 1987. p. 183. [P].
[36] Stocker ME, Korcber GW, Gassler G, Gudehus G. Soil nailing. International Conference on Soil Reinforcement,Paris, V. 2; 1979. p. 469-74.
[37] CALTRANS SNAIL Computer Program, Version 2.06: California Department of Transportation, Office of Geotechnical Engineering, Sacramento,California; 1993.
[38] Meenal G, Saran S, Mittal S. Pseudo-static analysis of soil nailed excavations. Geotech Geol Eng 2009;27:571–83.